Organization and Structure of Clouds and Precipitation on the Mid-Atlantic Coast of the United States. Part V: The Role of an Upper-Level Front in the Generation of a Rainband

JONATHAN E. MARTIN, JOHN D. LOCATELLI, AND PETER V. HOBBS

Atmospheric Sciences Department, University of Washington, Seattle, Washington

(Manuscript received 14 February 1991, in final form 22 July 1991)

ABSTRACT

The origins of a rainband of moderate intensity that occurred over the eastern Carolinas is investigated. It is concluded that the band formed in the updraft portion of a thermodynamically direct vertical circulation about an upper-level frontal zone in a region of conditional symmetrical instability (CSI). The release of CSI is presumed to have been responsible for the dimensions of the band and its orientation relative to the shear vector. An adiabatic mechanism for destabilization of the environment of the upper-level front to CSI was explored but found to be insignificant in this case.

1. Introduction

Upper-level fronts[1] have been discussed since Reed and Sanders (1953) and Reed (1955) documented their existence. They have been shown to be associated with synoptic-scale stratosphere–troposphere exchange processes (Danielson 1968), turbulent production of potential vorticity (Shapiro 1976; Keyser and Rotunno 1990), and rapid cyclogenesis (Uccellini et al. 1985). However, to our knowledge, it has not been shown previously that upper-level fronts and upper-level frontogenetic processes can produce precipitation bands. In this paper we present documentation of such a case.

We begin by presenting observational evidence for the existence of the upper-level front with which we are concerned here and the synoptic setting in which it developed. This will involve a discussion of upper-level frontogenesis in terms of the Sawyer (1956)–Eliassen (1962) diagnostic equation. Emphasis will be placed upon the products of the forced frontal circulation as they bear directly on the subsequent development of the precipitation band. We then describe some important characteristics of the precipitation band. Finally, the mesoscale environment in which the precipitation band developed is assessed to determine whether or not a mesoscale instability associated with the upper-level front produced the band.

2. Observations

A deep long-wave trough over the eastern two-thirds of the United States was the major feature in the North American 500-mb analysis at 1200 UTC 26 January 1986 (Fig. 1a). A rather broad region of synoptic-scale lifting was present east of the trough axis, as indicated by the IR satellite image for that time (Fig. 1b), and the Nested Grid Model (NGM) 12-h forecast for 500-mb vertical velocities valid at 1200 UTC 26 January (Fig. 1c). The trough had a large horizontal temperature gradient along its entire eastern side. The position of the baroclinic zone in northern Georgia and South Carolina was located just downstream of a zone of rather vigorous frontogenetic horizontal confluence (Fig. 1d).

Within the region of widespread large-scale lifting, various precipitating features were present at 1200 UTC 26 January. In Fig. 2, a manually digitized National Weather Service (NWS) radar summary of these features is overlayed on the surface frontal analysis for 1200 UTC. Some of the precipitation features are easily identified with weather features (e.g., the surface front in the Gulf of Mexico, the shallow coastal front along the northeastern United States coast, and the weak low pressure system that was developing along the coastal front). However, the rainband located in extreme northeastern South Carolina did not appear to be associated with any surface feature. Close examination of the data taken by the triad of NWS radars located at Cape Hatteras (HAT) and Wilmington (ILM), North Carolina, and Volens (VQN), Virginia, showed that the precipitation cells in this rainband were moving

[1] We use the term "upper-level front" to refer to a front generated in the vicinity of the tropopause of the type discussed by Keyser and Shapiro (1986). They should not be confused with "cold fronts aloft" of the type discussed by Hobbs et al. (1990), which occur lower down in the troposphere.

Corresponding author address: Dr. Peter V. Hobbs, Department of Atmospheric Sciences AK-40, University of Washington, Seattle, WA 98195.

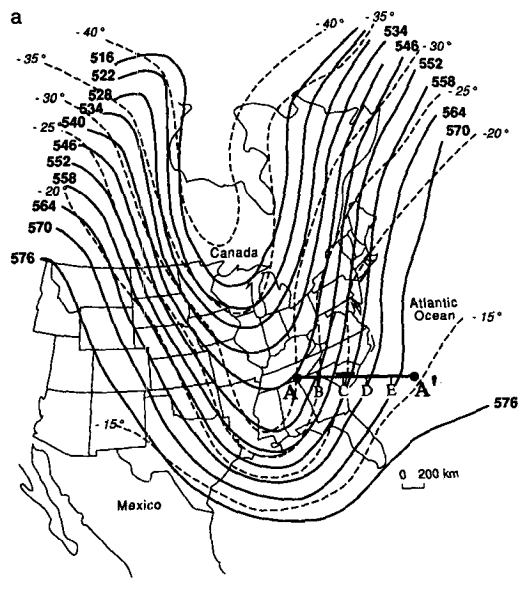

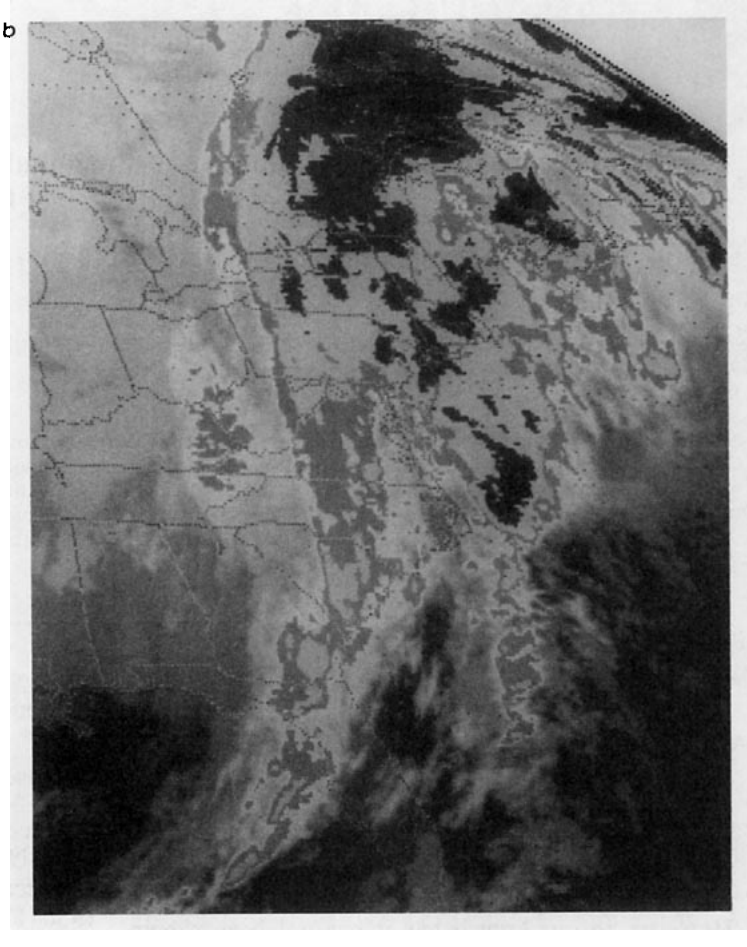

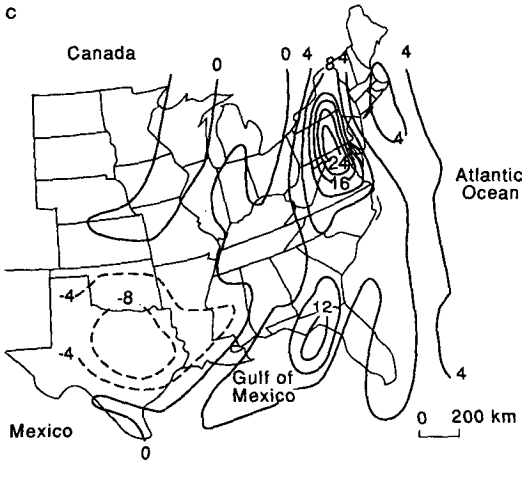

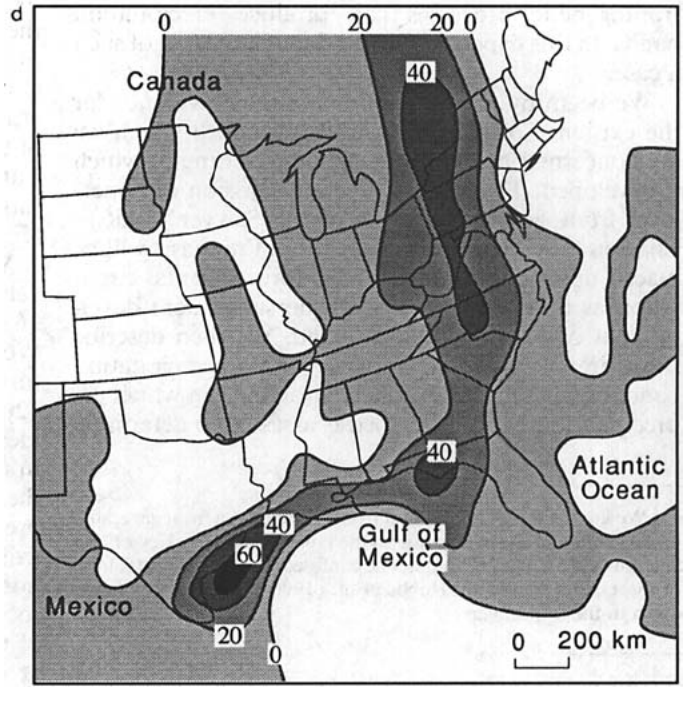

FIG. 1. (a) NMC's North American 500-mb analysis for 1200 UTC 26 January 1986. Shown are geopotential heights (continuous lines, labeled in tens of meters and contoured every 60 m) and temperatures (dashed lines, labeled in °C and contoured every 5°C). A cross section along line A–A is shown in Fig. 7. (b) Infrared satellite image for 1200 UTC 26 January 1986. (c) 12-hour forecast of the vertical velocity field at 500 mb valid at 1200 UTC 26 January 1986 from NMC's Nested Grid Model. Shown are the contours of upward vertical velocity (continuous lines, labeled in cm s^{-1} and contoured every 4 cm s^{-1}) and downward vertical velocity (dashed lines, labeled in cm s^{-1} and contoured every 4 cm s^{-1}). (d) Confluent frontogenesis

$$F_{2C} = \frac{1}{|\nabla\theta|}\left[-\frac{\partial\theta}{\partial x}\left(\frac{\partial u}{\partial x}\frac{\partial\theta}{\partial x}\right) - \frac{\partial\theta}{\partial y}\left(\frac{\partial v}{\partial y}\frac{\partial\theta}{\partial y}\right)\right]$$

at 500 mb at 1200 UTC 26 January 1986 calculated using the NGM initialized data at 1200 UTC. Positive values labeled in K m^{-1} s^{-1} and contoured every 20×10^{-11} K m^{-1} s^{-1}.

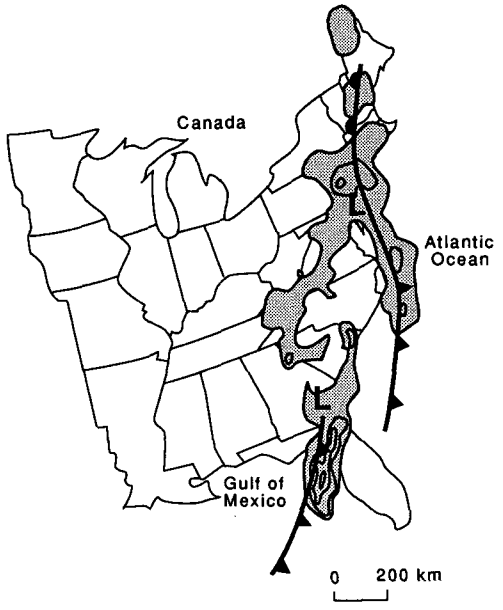

FIG. 2. Manually digitized NWS radar summary (shaded area) at 1200 UTC 26 January 1986. Outermost contour value is 1 dBZ. Successive contour intervals are 12, 24, and 36 dBZ. Authors' analysis of surface low pressure centers and surface frontal positions are overlaid.

at the velocity of the winds at ~550 mb (as determined by comparison with a local sounding). We surmise, therefore, that the precipitation cells were being generated at this level. Therefore, it was possible that the rainband was associated with frontogenetic processes at midtropospheric levels. Tracking of this rainband indicated that it maintained its association with the upper-level baroclinic feature throughout its life cycle of approximately 6 hours. This is the rainband with which we are concerned. Since frontogenesis in the middle troposphere appeared to be directly linked to the production of this rainband, we will first trace the evolution of this baroclinic zone.

a. Development of the upper-level frontal zone

Figure 3 shows the 500-mb charts for 1200 UTC 24 January, 0000 and 1200 UTC 25 January, and 0000 UTC 26 January 1986. At 1200 UTC 24 January (Fig. 3a), Spokane (GEG), Washington, had an isolated wind-speed maxima of 37 m s^{-1} in an otherwise straight flow over the Pacific Northwest. By 0000 UTC 25 January (Fig. 3b) that isolated wind maxima had moved to central Wyoming and developed into a shortwave disturbance characterized by both shear and curvature vorticity. Also, an increase in the temperature gradient occurred over the intervening 12 h (from a maximum of 2.165 K/100 km at 1200 UTC to 2.747 K/100 km at 0000 UTC 25 January). By 1200 UTC 25 January (Fig. 3c), a jet of greater meridional extent had developed simultaneously with a further intensification of the temperature gradient across it, which had a maximum value of 2.879 K/100 km at 1200 UTC. By 0000 UTC 26 January a wind maximum of 45 m s^{-1}, embedded within a thin jet streak stretching from Colorado through Texas, was entering the base of the long-wave trough over the eastern United States (Fig. 3d). A cross section at 0000 UTC 26 January along line B–B′ in Fig. 3d from Monett (UMN), Missouri, to Oklahoma City (OKC), Oklahoma, to Stephenville (SEP), Texas, to Midland (MAF), Texas, is shown in Fig. 4. This cross section clearly depicts an upper-level frontal zone.

As we shall see later, the manner in which this frontal zone formed affected the environment of the rainband. Therefore, we will now use the Sawyer–Eliassen diagnostic equation to gain insight into the formation process. This 2D equation can be used to diagnose the transverse vertical circulation that must accompany frontogenesis. It combines the alongfront momentum equation and the conservation of potential temperature, subject to the assumptions of across-front geostrophic balance and the geostrophic momentum approximation (i.e., $dU/dt = dU_g/dt$, where U and U_g are the actual horizontal wind and geostrophic wind, respectively, along the front). This assumption is less restrictive than the pure geostrophic assumption (Hoskins 1975). Only across-front and vertical ageostrophic advection of the geostrophic wind and temperature are considered in the Sawyer–Eliassen equation; alongfront ageostrophy is assumed insignificant.

The resulting equation is a linear, second-order, partial differential equation with variable coefficients that describe the streamfunction of the transverse secondary circulation accompanying frontogenesis. In the absence of friction, this circulation is described by the following equation:

$$-\gamma\frac{\partial\theta}{\partial y}\left(\frac{\partial^2\psi}{\partial y^2}\right)+2\gamma\frac{\partial\theta}{\partial y}\left(\frac{\partial^2\psi}{\partial p\partial y}\right)-\left(\frac{\partial U_g}{\partial y}-f\right)\left(\frac{\partial^2\psi}{\partial p^2}\right)$$
$$=Q=2\gamma\underbrace{\left(\frac{\partial U_g}{\partial y}\frac{\partial\theta}{\partial x}\right)}_{\text{(A)}}-\underbrace{\frac{\partial U_g}{\partial x}\frac{\partial\theta}{\partial y}}_{\text{(B)}}-\underbrace{\gamma\frac{\partial\dot\theta}{\partial y}}_{\text{(C)}} \quad (1)$$

where

$$\gamma=\frac{R}{fp_0}\left(\frac{p_0}{p}\right)^{c_v/c_p},\quad \dot\theta=\frac{d\theta}{dt},$$
$$v_a=-\frac{\partial\psi}{\partial p},\quad\text{and}\quad \omega=\frac{\partial\psi}{\partial y} \quad (2)$$

and θ is the potential temperature, v_a and ω are the y and p ageostrophic winds, respectively, and the y axis is positive pointing into the cold air. Term A in (1) is the contribution from geostrophic shearing deformation, term B the geostrophic confluence, and term C the diabatic heating. As discussed in detail by Keyser

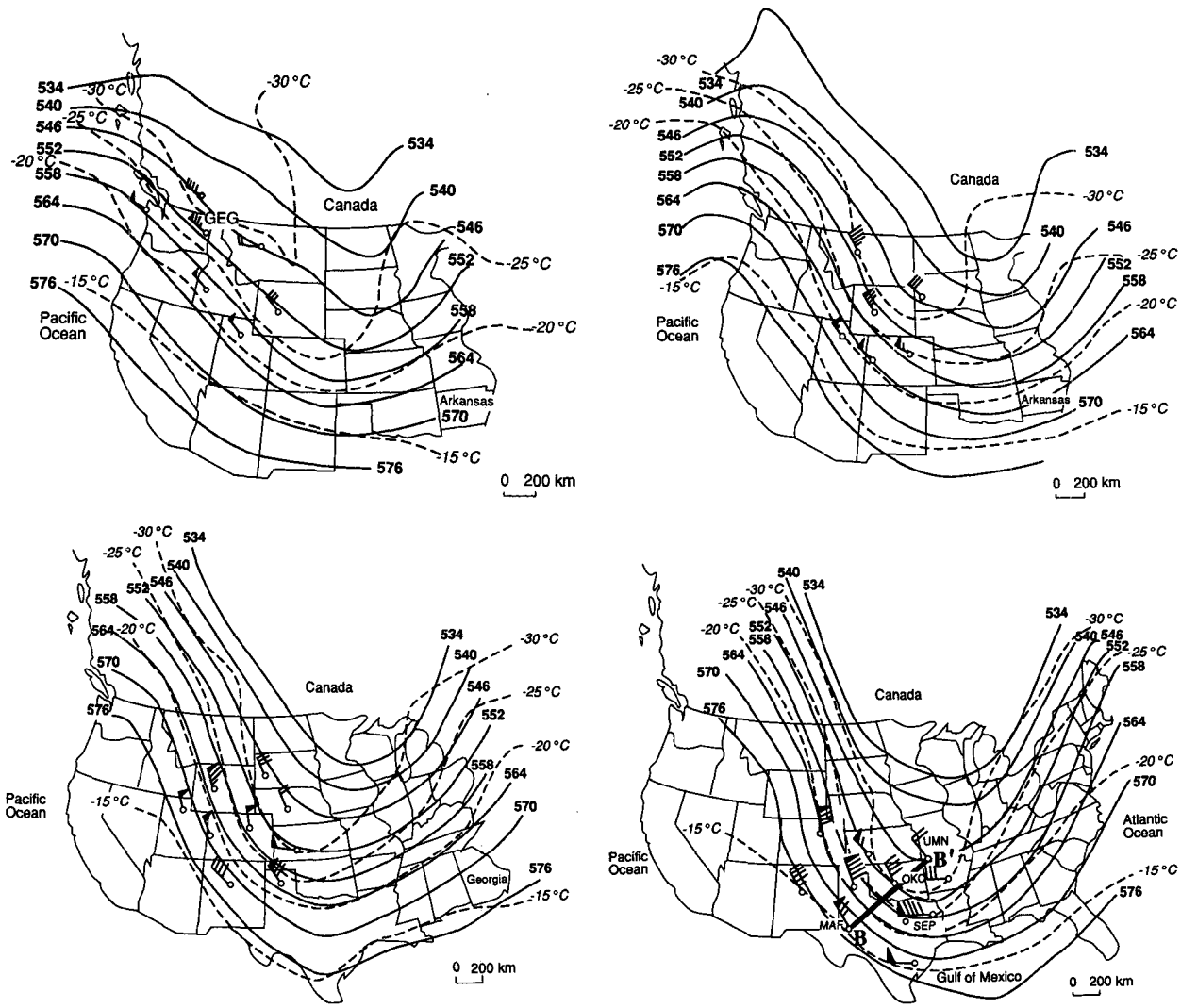

FIG. 3. (a) As for Fig. 1a, except for 1200 UTC 24 January 1986 with wind speed indicated by flag: 25 m s^{-1}, long barb: 5 m s^{-1}, and short barb: 2.5 m s^{-1}. (b) As for (a), except for 0000 UTC 25 January 1986. (c) As for (a), except for 1200 UTC 25 January 1986. (d) As for (a), except for 0000 UTC 26 January 1986. A cross section along line B–B′ is shown in Fig. 4.

and Shapiro (1986), a positive (negative) Q results in a thermodynamically direct (indirect) vertical circulation, that is, warm air rising (sinking) and cold air sinking (rising).

Analysis of the geostrophic portion of Q for the cross section shown in Fig. 4 showed that Q was negative aloft (Fig. 5a) and that this was almost entirely due to the shearing term (Fig. 5b). This term is negative if cold air advection along the front occurs in the presence of cyclonic shear. Referring back to Fig. 3, it appears that such a process was acting to intensify this frontal zone throughout its history. Thus, a thermodynamically indirect, frontogenetic, vertical circulation developed.

The consequences of this frontogenetic circulation are: 1) an increase in the horizontal temperature gradient, 2) an increase in the relative vorticity produced by transforming vertical shear into the horizontal via differential vertical motions, 3) advection of stratospheric air into the troposphere, and 4) creation of a large reservoir of adiabatically dried (i.e., low relative humidity) air along the warm edge of the frontal zone.

At 1200 UTC, the upper-level frontal zone was just moving into South Carolina, although in a weakened state. Figure 6 shows an isentropic cross section at 1200 UTC along line A–A′ in Fig. 1a. Differential advection in a horizontal deformation field leads to a thermodynamically direct vertical circulation by concentrating the horizontal temperature gradient. This, in turn, induces accelerations along the front. Therefore, it is relatively simple to infer the location of vertical circulations and frontal positions by locating regions where

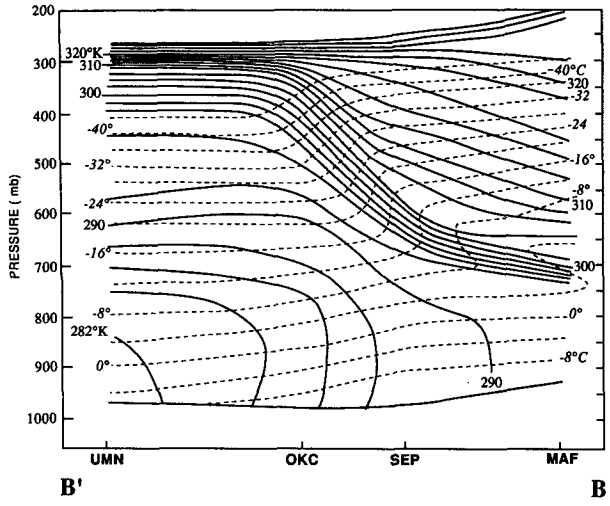

FIG. 4. Cross section from Monett (UMN), Missouri, to Oklahoma City (OKC), Oklahoma, to Stephenville (SEP) to Midland (MAF), Texas, along line B–B′ in Fig. 3d. Solid lines are isentropes labeled in K and contoured every 2 K. Dashed lines are temperatures (in °C) contoured every 4°C.

the horizontal flow (in this case, on isobaric surfaces) acts to concentrate the horizontal temperature gradient. The Sawyer–Eliassen equation represents this forcing in a highly idealized manner by considering only the geostrophic stretching and shearing deformations. A more complete picture is obtained by using the full wind. Therefore, we calculated a frontogenesis function:

$$F_2 = \frac{d}{dt}|\nabla\theta| = \frac{\partial}{\partial t}|\nabla\theta| + \mathbf{V}_2\cdot\nabla_2|\nabla\theta|,$$

where $\mathbf{V}_2$ and ∇_2 are the 2D (x, y) total wind and gradient operator, respectively. For adiabatic conditions,

$$F_2 = \frac{1}{|\nabla\theta|}\left[-\frac{\partial\theta}{\partial x}\left(\frac{\partial u}{\partial x}\frac{\partial\theta}{\partial x}+\frac{\partial v}{\partial x}\frac{\partial\theta}{\partial y}\right) - \frac{\partial\theta}{\partial y}\left(\frac{\partial u}{\partial y}\frac{\partial\theta}{\partial x}+\frac{\partial v}{\partial y}\frac{\partial\theta}{\partial y}\right)\right].$$

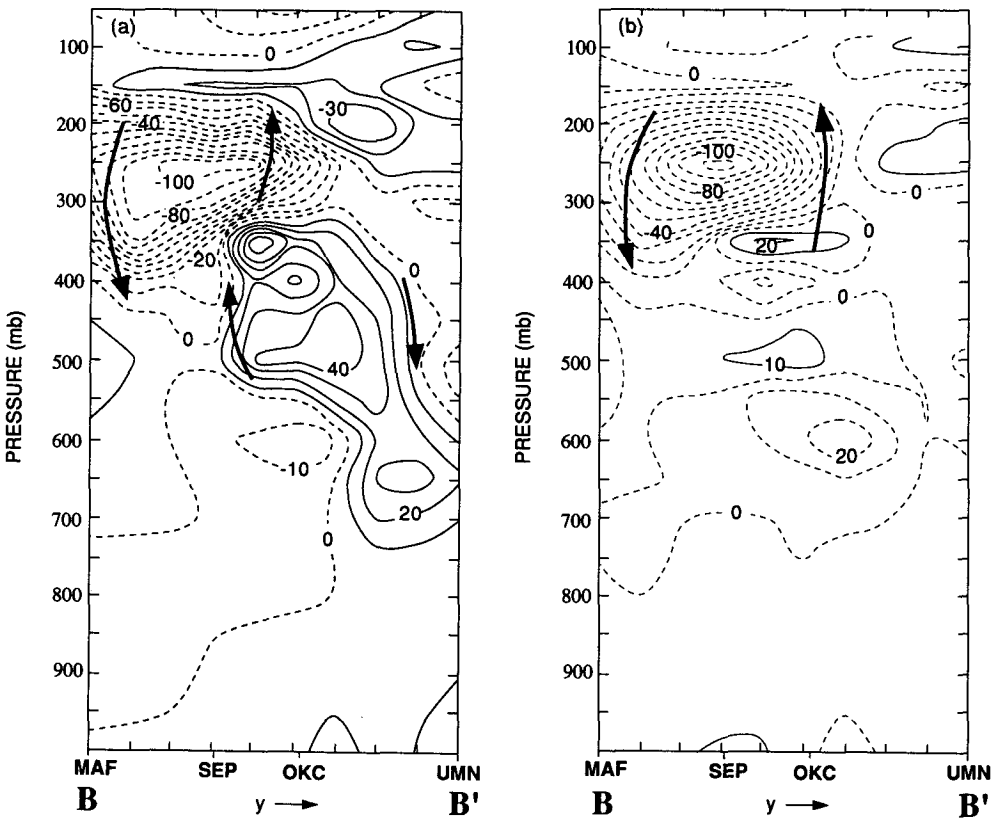

FIG. 5. (a) Cross section of total geostrophic Q forcing [terms A and B in (1)] of the secondary circulation along line B–B′ calculated from NGM initialized data at 0000 UTC 26 January 1986. Dashed lines are negative values labeled in $m^2\ kg^{-1}$ and contoured every $10 \times 10^{-8}\ m^2\ kg^{-1}$; solid lines are positive values and follow the same convention. Bold arrows indicate the sense of the forced vertical circulation. (b) Cross section of shearing deformation forcing [term A in (1)] of the secondary circulation along line B–B′ at 0000 UTC 26 January 1986. Contouring and symbols as for Fig. 5a.

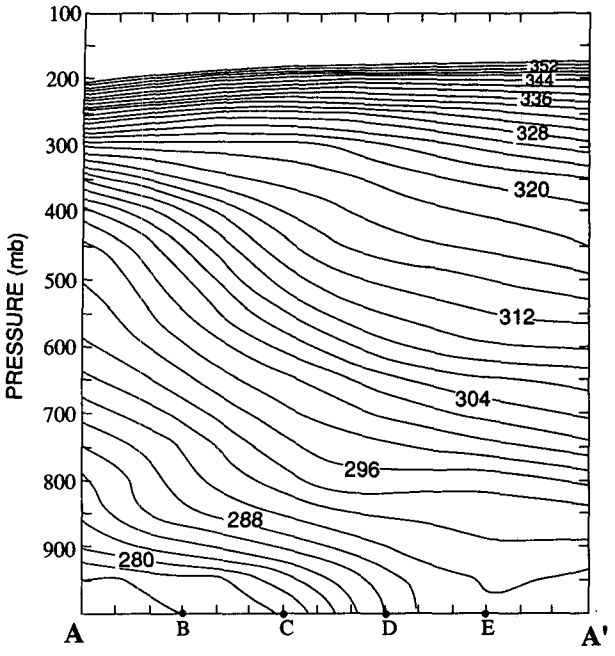

FIG. 6. NGM cross section along line A–A′ in Fig. 1a at 1200 UTC 26 January 1986. Lines are isentropes labeled in K and contoured every 2 K. Letters B–C–D–E are spaced at 240-km intervals.

Values of F_2 were calculated along A–A′ using the NGM initialized dataset at 1200 UTC 26 January. Although this frontogenesis function ignores the modifying effect of vertical velocity on gradient strength, it clearly reveals the region and circumstances for the forcing of vertical circulations. Shown in Fig. 7 are the F_2 values in a cross section along A–A′ at 1200 UTC. The sense of the induced circulation is also indicated. The rainband with which we are concerned here formed in the upward branch of this frontal circulation.

b. *The rainband*

Figure 8 shows the hourly positions of the rainband from 1200 to 1500 UTC 26 January derived from the radars indicated in the figure. Figure 8a also includes the 700–300-mb thickness contours at 1200 UTC. The rainband was oriented along the thermal wind vector associated with the upper-level front. The band was only ~20–40 km wide, which suggests that a narrow, intense updraft, aligned along the shear vector, was responsible for its generation.

These observations are consistent with theoretical expectations if the rainband was produced by the release of conditional symmetric instability (CSI), which is a 2D mesoscale instability in which both gravitational and inertial buoyancy determine the displacement of an air parcel (Bennetts and Hoskins 1979). Assuming that no variations exist in the along-shear (y) direction, it can be shown (e.g., Emanuel 1983) that horizontal and vertical accelerations of a saturated parcel can be related to the absolute momentum (M) and equivalent potential temperature (θ_e) of the parcel relative to the environment. Thus,

$$\frac{dU}{dt} \propto (M_p - M_E) \tag{3}$$

$$\frac{dw}{dt} \propto (\theta_{ep} - \theta_{eE}), \tag{4}$$

where the subscripts p and E refer to parcel and environmental values, respectively, and $M = v + fx$, where v is the along-shear wind speed, f is the Coriolis parameter, and x is positive in the across-shear direction toward warm air.

For the schematic shown in Fig. 9, a saturated parcel displaced along the slanted path S–S′ would continue to accelerate in that direction and, therefore, be unstable to such a displacement. As is evident from Fig. 9, an environment that is stable to purely vertical and purely horizontal displacement can be unstable to slantwise displacement. By simple energy considerations, it can be shown that an environment is unstable to saturated slantwise displacements if $(\partial M/\partial x)_{\theta_e} < 0$, that is, if the θ_e surfaces are steeper than the M surfaces (as in Fig. 9). In 2D flow, this is identical to the equivalent potential vorticity (P_e) being negative. This follows from the definition of P_e:

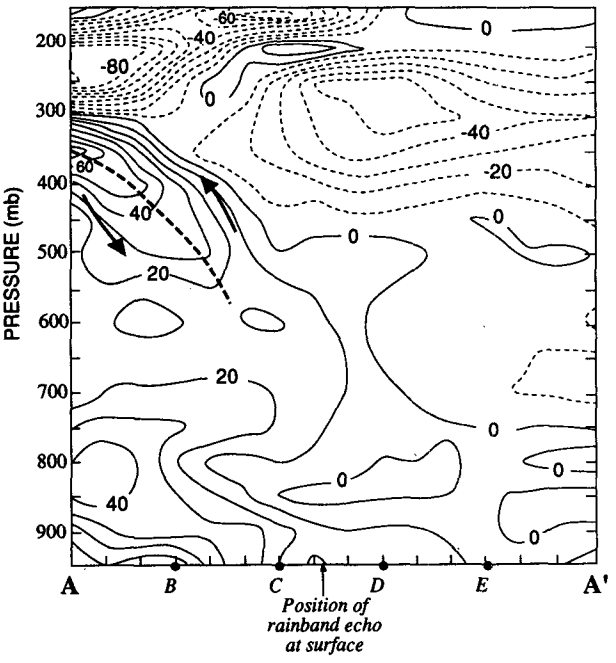

FIG. 7. Values of F_2 (in K m^{-1} s^{-1} and contoured every 10×10^{-11} K m^{-1} s^{-1}) along A–A′ in Fig. 1a at 1200 UTC 26 January 1986. The solid and dashed contours indicate positive and negative values of F_2, respectively. The heavy dashed line shows the axis of maximum F_2, and the arrows indicate the sense of the induced vertical circulation. Letters B–C–D–E are spaced at 240-km intervals.

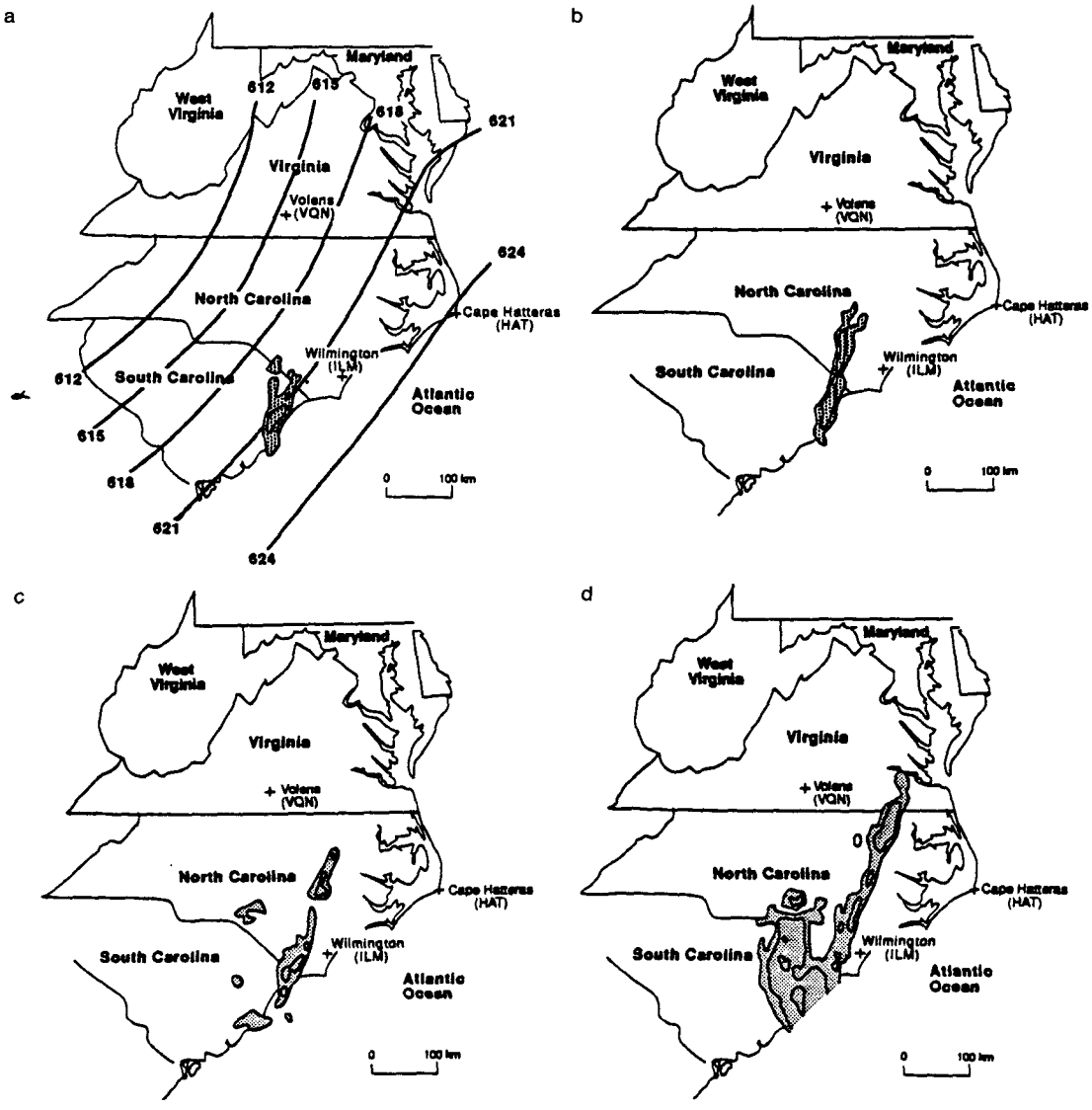

FIG. 8. (a) NWS radar mosaic of rainband at 1200 UTC 26 January 1986. Radar dBZ levels (shaded region) contoured as in Fig. 2. Contours represent 700–300-mb thickness at 1200 UTC (labeled in tens of meters and contoured every 30 m). Panels (b)–(d) for 1300 UTC, 1400 UTC, and 1500 UTC 26 January 1986, respectively, but without thickness analysis.

$$P_e = -\boldsymbol{n}\cdot\nabla\theta_e,$$

where $\boldsymbol{n}$ is the 3D absolute vorticity and ∇ the gradient operator in x, y, and p coordinates. Neglecting y variations and the contribution to $\boldsymbol{n}$ from terms involving $\omega\,(=dp/dt)$, we obtain

$$P_e = \frac{\partial v}{\partial p}\frac{\partial \theta_e}{\partial x} - \left(\frac{\partial v}{\partial x} + f\right)\frac{\partial \theta_e}{\partial p},$$

or since $M = v + fx$,

$$P_e = \frac{\partial M}{\partial p}\frac{\partial \theta_e}{\partial x} - \frac{\partial M}{\partial x}\frac{\partial \theta_e}{\partial p},$$

which is negative for the situation portrayed in Fig. 9, since the first term on the right-hand side dominates.

In a modeling study, Thorpe and Emanuel (1985) showed that the circulation produced by a given frontogenetic forcing is sensitive to across-front differences in the slantwise stability. When the slantwise stability is lower on the warm, saturated side of the front [i.e., when the (equivalent) potential vorticity is lower on the warm side], a vigorous, horizontally restricted updraft occurs in that air mass while a gentle, widespread downdraft occurs in the colder, drier air behind the front. Theoretically, this is because the (equivalent) potential vorticity, being a measure of slantwise stability, plays an analogous role in the Sawyer–Eliassen equation to that played by static stability in the quasigeostrophic omega equation; where the (equivalent) potential vorticity is small, the response is large, and

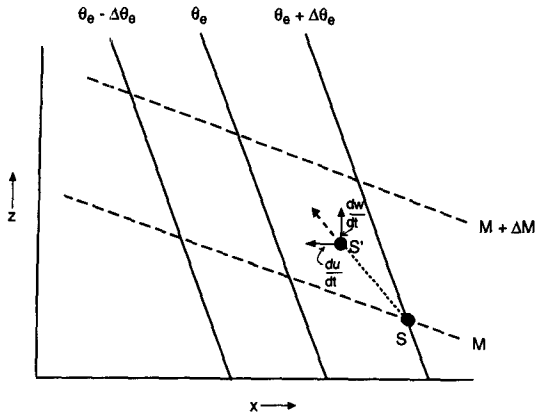

FIG. 9. Schematic illustrating an atmospheric structure susceptible to conditional symmetric instability (CSI). Solid lines are contours of equivalent potential temperature (θ_e). Dashed lines are contours of pseudo-absolute momentum (M). S–S′ is the path of a hypothetically displaced, saturated parcel.

vice versa. In order for mass balance to be maintained across the front, the vigorous updraft must be horizontally restricted, leading to its manifestation as a thin, banded precipitating feature. Sanders and Bosart (1985) explained a long-lived snowband in an East Coast snowstorm as the result of low slantwise stability in the saturated air on the warm side of a frontogenetic circulation, and Moore and Blakely (1988) considered a similar circumstance to be the formative mechanism for a narrow band of heavy snow that fell in a Midwest winter cyclone.

To further assess the likelihood of CSI as a mechanism for the formation of the rainband being discussed here, we used the NGM initialized data at 1200 UTC 26 January to construct a series of cross sections along the line A–A′ in Fig. 1a. This line is just upstream of the 1200 UTC radar observation of the rainband. Using typical fall speeds for frozen and liquid precipitation and taking into account the ambient shear, the double line (in the vicinity of point C) along A–A′ in Fig. 1a represents the most likely origin of the precipitation particles observed by the Wilmington (ILM) radar scanning at near 0° zenith angle. This line is indicated by the 2D box in the cross sections shown in Fig. 10.

Figure 10a shows the M and θ_e lines along A–A′ at 1200 UTC 26 January. Conditional symmetric instability exists in the stippled regions, since there the θ_e lines are steeper than the M lines. Notice that the low-level region of CSI over the Gulf Stream is also a region of convective instability (a special case of the more general CSI). The larger region at midlevels, which is not convectively unstable anywhere, includes the 2D box representing the likely generation region for the rainband. Figure 10b shows the relative humidity (RH) from the NGM along the same cross section. In the NGM 95% RH is considered to be saturation, and regions with higher RH are assumed to be cloudy. There is a region of saturation in the CSI area at about 700 mb, but the rainband did not form at this low level. Within the 2D box the RH was high and, at the ambient temperatures, needed to be lifted only slightly to reach saturation. Figure 10c shows the 12-h forecast of vertical velocity, valid at 1200 UTC, along the same section. The area of saturation at 700 mb is subject to weak downward motion on its western side and only slight upward motion on its eastern side. Within the 2D box there was significant upward motion (up to 6 cm s^{-1}), which we attribute to the confluent frontogenetic flow along the upper-level front. The curvature of the flow far upstream (400–600 km) of the proposed region of generation of the rainband likely added to the magnitude of the vertical motion through some induced along-flow ageostrophy. However, this region was remote enough from the curvature variations to warrant consideration of the horizontal frontogenetic flow as the overwhelming influence on the observed vertical motion in the rainband generation region. Thus, the region within the 2D box was characterized by CSI, nearly saturated air, and significant vertical motion.

In view of the above analysis and the physical dimensions of the band and its orientation relative to the shear vector, we conclude that the rainband was formed by the release of CSI in the updraft portion of a thermally direct circulation about an upper-level frontal zone.

c. *Formation and evolution of the environment of the rainband*

As noted previously, for 2D flows there is an equivalence between regions of negative equivalent potential vorticity (P_e) and regions of CSI. Since the frontal zone along which the rainband formed was essentially a 2D feature, we will use this equivalence to explore the evolution of the environment of the rainband.

The first step in this process is to determine the Lagrangian derivative of P_e. In pressure coordinates

$$P_e = -(f\tilde{k} + \nabla \times \mathbf{V}) \cdot \nabla_3 \theta_e, \tag{5}$$

where ∇_3 is the 3D gradient operator $[(\partial/\partial x)\tilde{i}, (\partial/\partial y)\tilde{j}, (\partial/\partial p)\tilde{k}]$.
Hence,

$$\frac{dP_e}{dt} = -\boldsymbol{n} \cdot \nabla_3 \dot{\theta}_e + f \frac{\partial \mathbf{V}_g}{\partial p} \cdot \nabla_2 \theta_e, \tag{6}$$

(A) (B)

where ∇_2 is the 2D gradient operator, $\boldsymbol{n}$ the 3D vorticity vector, and $\dot{\theta}_e$ ($= d\theta_e/dt$) the diabatic heating rate (see Bennetts and Hoskins 1979). In addition to diabatically driven changes in P_e [term A in (6)], there exists, as pointed out by Bennetts and Hoskins (1979) and

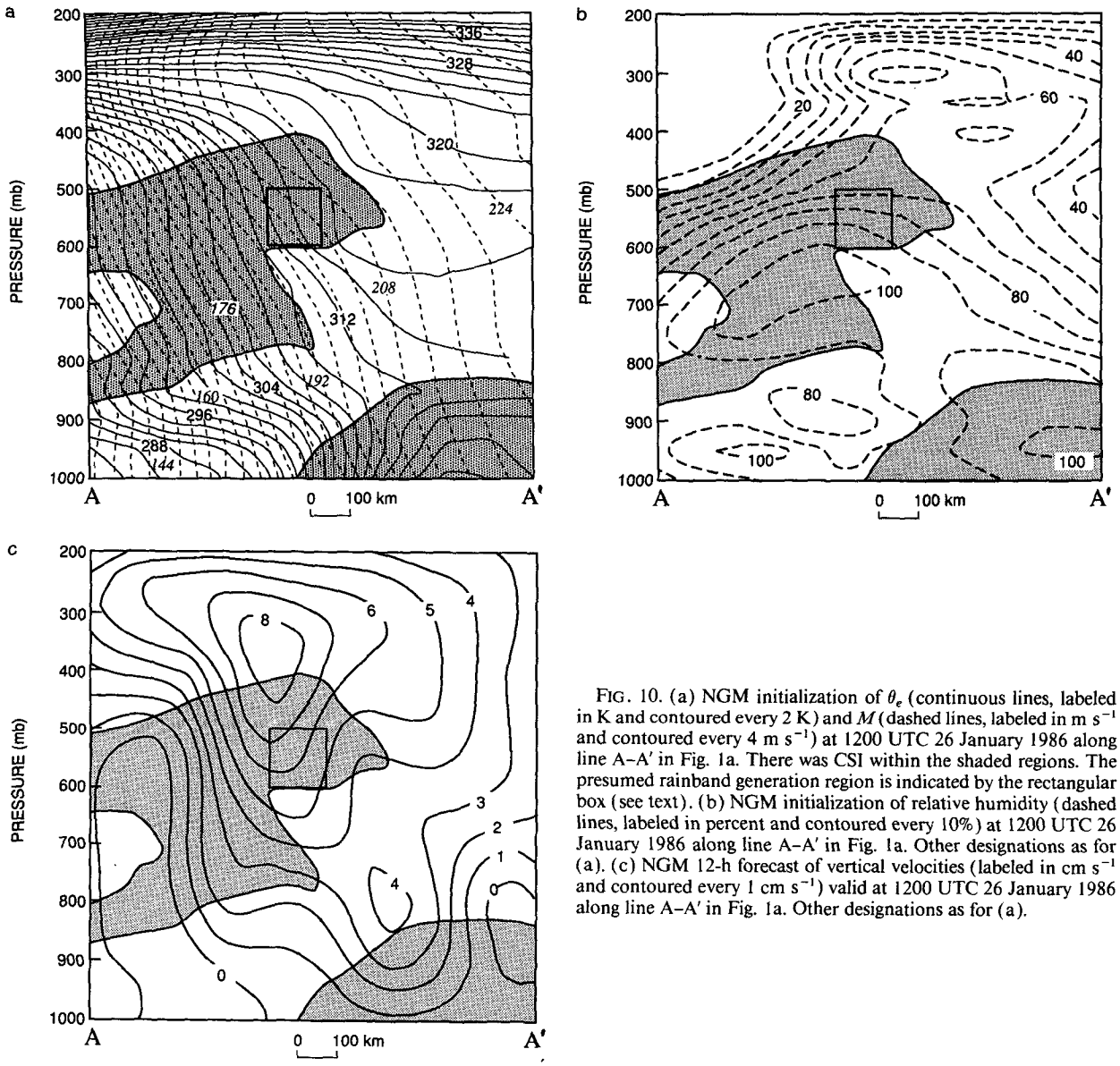

FIG. 10. (a) NGM initialization of θ_e (continuous lines, labeled in K and contoured every 2 K) and M (dashed lines, labeled in m s^{-1} and contoured every 4 m s^{-1}) at 1200 UTC 26 January 1986 along line A–A′ in Fig. 1a. There was CSI within the shaded regions. The presumed rainband generation region is indicated by the rectangular box (see text). (b) NGM initialization of relative humidity (dashed lines, labeled in percent and contoured every 10%) at 1200 UTC 26 January 1986 along line A–A′ in Fig. 1a. Other designations as for (a). (c) NGM 12-h forecast of vertical velocities (labeled in cm s^{-1} and contoured every 1 cm s^{-1}) valid at 1200 UTC 26 January 1986 along line A–A′ in Fig. 1a. Other designations as for (a).

Thorpe and Clough (1991), an adiabatic process by which P_e may be changed, namely, by the advection of moisture along the front by the thermal wind [term B in (6)]. Thermal wind "advection" of dry (moist) air along the front decreases (increases) P_e, thereby affecting the CSI of the parcel.

One of the by-products of the upper-level frontogenetic process in the case under discussion here was the creation of an enormous pool of dry air on the warm side of the front in the middle troposphere (Fig. 11). This dry pool was a potential source of strongly negative adiabatic forcing of P_e. To determine whether the rainband environment was made conditionally symmetrically unstable due to such adiabatic forcing, we calculated backward trajectories from the rainband using 6-h and 12-h forecast data from the NGM. This analysis showed that for the case under discussion here, although there was a decrease in the moist slantwise stability of parcels streaming toward the generation region of the rainband, this decrease was not due to adiabatic destabilization. Diabatic processes, such as cloud-top radiative cooling, may have been responsible; however, the dataset available does not permit quantitative evaluation of such effects.

3. Conclusions

In this paper we have shown that a rainband of moderate intensity was generated through the release

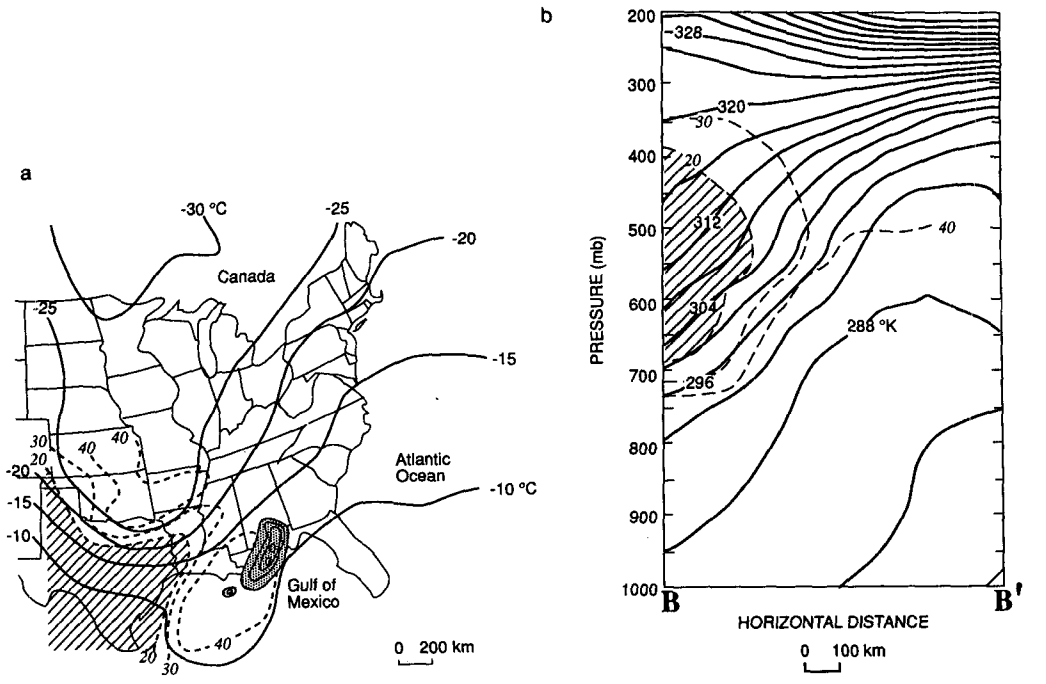

FIG. 11. (a) 500-mb temperature (continuous lines, labeled in °C and contoured every 5°C) and relative humidity (dashed lines, labeled in percent; the hatched region indicates RH < 20%) from NGM initialization at 0000 UTC 26 January. Manually digitized radar depiction of the convective line in the Gulf of Mexico at 0000 UTC is shown by the shaded area with reflectivities contoured as for Fig. 2. (b) Vertical cross section along B–B' in Fig. 3d at 0000 UTC 26 January 1986 from NGM initialization. Indicated are potential temperature (continuous lines, labeled in K and contoured every 4 K) and relative humidity (dashed lines, labeled in percent with hatched region indicating RH < 20%).

of CSI in the saturated updraft portion of a thermally direct circulation about an upper-level frontal zone. To our knowledge, this is the first time that a rainband has been shown to be produced by an upper-level front (see footnote 1). The upper-level frontogenetic process created a large pool of dry air at the warm edge of the frontal zone. This strong moisture gradient along the front, coupled with strong vertical shear, served to dramatically decrease the equivalent potential vorticity of air parcels originating immediately downstream of the dry pool. However, the environment of the rainband was apparently not made conditionally symmetrically unstable by this process; diabatic processes may have been responsible.

The synoptic ingredients involved in this case study are not rare, neither did they act with unusual vigor. Indeed, in the eastern United States similar conditions are rather common. Consequently, we hypothesize that upper-level fronts may often produce rainbands. The upper-level frontogenetic process may also exert a significant influence on the stability characteristics of the environment that affects rainband formation. More accurate and temporally dense observational and numerical modeling data will be needed for more detailed investigations of this phenomenon.

Acknowledgments. This material is based on work supported by the National Science Foundation under Grant ATM-8810650. The government has certain rights in this material.

REFERENCES

Bennetts, D. A., and B. J. Hoskins, 1979: Conditional symmetric instability—A possible explanation for frontal rainbands. *Quart. J. Roy. Meteor. Soc.*, **105,** 945–962.

Danielsen, E. F., 1968: Stratospheric–tropospheric exchange based on radioactivity, ozone and potential vorticity. *J. Atmos. Sci.*, **25,** 502–518.

Eliassen, A., 1962: On the vertical circulation in frontal zones. *Geofys. Publ.*, **24,** 147–160.

Emanuel, K. A., 1983: Lagrangian parcel dynamics of moist symmetric instability. *J. Atmos. Sci.*, **40,** 2368–2376.

Hobbs, P. V., J. D. Locatelli, and J. E. Martin, 1990: Cold fronts aloft and the forecasting of precipitation and severe weather east of the Rocky Mountains. *Wea. Forecasting,* **5,** 613–626.

Hoskins, B. J., 1975: The geostrophic momentum approximation and the semi-geostrophic equations. *J. Atmos. Sci.*, **32,** 233–242.

Keyser, D., and M. A. Shapiro, 1986: A review of the structure and dynamics of upper level frontal zones. *Mon. Wea. Rev.*, **114,** 452–499.

——, and R. Rotunno, 1990: On the formation of potential vorticity anomalies in upper level jet-front systems. *Mon. Wea. Rev.*, **118,** 1914–1921.

Moore, J. T., and P. D. Blakely, 1988: The role of frontogenetic forcing and conditional symmetric instability in the Midwest snowstorm of 30–31 January 1982. *Mon. Wea. Rev.*, **116,** 2155–2171.

Reed, R. J., 1955: A study of a characteristic type of upper-level frontogenesis. *J. Meteor.*, **12,** 36–42.

——, and F. Sanders, 1953: An investigation of the development of a midtropospheric frontal zone and its associated vorticity field. *J. Meteor.*, **10,** 338–349.

Sanders, F., and L. F. Bosart, 1985: Mesoscale structure in the megalopolitan snowstorm of 11–12 February 1983. Part I: Frontogenetical forcing and symmetric instability. *J. Atmos. Sci.*, **42,** 1050–1061.

Sawyer, J. S., 1956: The vertical circulation at meteorological fronts and its relations to frontogenesis. *Proc. Roy. Soc. London,* **A234,** 346–362.

Shapiro, M. A., 1976: The role of turbulent heat flux in the generation of potential vorticity in the vicinity of upper-level jet stream systems. *Mon. Wea. Rev.*, **104,** 892–906.

Thorpe, A. J., and K. A. Emanuel, 1985: Frontogenesis in the presence of small stability to slantwise convection. *J. Atmos. Sci.*, **42,** 1809–1824.

——, and S. A. Clough, 1991: Mesoscale dynamics of cold fronts: Structures described by dropsoundings in FRONTS 87. *Quart. J. Roy. Meteor. Soc.*, **117,** 903–941.

Uccellini, L. W., D. Keyser, K. F. Brill, and C. H. Wash, 1985: The Presidents' Day cyclone of 18–19 February 1979: Influence of upstream trough amplification and associated tropopause folding on rapid cyclogenesis. *Mon. Wea. Rev.*, **113,** 962–988.